Published in final edited form as:
Glia. 2011 July ; 59(7): 1009–1021. doi:10.1002/glia.21172.

Central nervous system dysfunction in a mouse model of FA2H deficiency

Kathleen A. Potter[1], **Michael J. Kern**[2], **George Fullbright**[1], **Jacek Bielawski**[1], **Steven S. Scherer**[3], **Sabrina W. Yum**[3], **Jian J. Li**[3], **Hua Cheng**[4], **Xianlin Han**[4,§], **Jagadish Kummetha Venkata**[1], **P. Akbar Ali Khan**[1], **Bärbel Rohrer**[5], and **Hiroko Hama**[1,*]

[1] Department of Biochemistry and Molecular Biology, Medical University of South Carolina, Charleston, South Carolina

[2] Department of Regenerative Medicine and Cell Biology, Medical University of South Carolina, Charleston, South Carolina

[3] Department of Neurology, University of Pennsylvania School of Medicine, Philadelphia, Pennsylvania

[4] Department of Internal Medicine, Washington University School of Medicine, St. Louis, Missouri

[5] Departments of Ophthalmology and Neurosciences, Medical University of South Carolina, Charleston, South Carolina

Abstract

Fatty acid 2-hydroxylase (FA2H) is responsible for the synthesis of myelin galactolipids containing hydroxy fatty acid (hFA) as the *N*-acyl chain. Mutations in the *FA2H* gene cause leukodystrophy, spastic paraplegia, and neurodegeneration with brain iron accumulation. Using the Cre-lox system, we developed two types of mouse mutants, $Fa2h^{-/-}$ mice (*Fa2h* deleted in all cells by germline deletion) and $Fa2h^{flox/flox}$ Cnp1-Cre mice (*Fa2h* deleted only in oligodendrocytes and Schwann cells). We found significant demyelination, profound axonal loss, and abnormally enlarged axons in the CNS of $Fa2h^{-/-}$ mice at 12 months of age, while structure and function of peripheral nerves were largely unaffected. $Fa2h^{-/-}$ mice also exhibited histological and functional disruption in the cerebellum at 12 months of age. In a time course study, significant deterioration of cerebellar function was first detected at 7 months of age. Further behavioral assessments in water T-maze and Morris water maze tasks revealed significant deficits in spatial learning and memory at 4 months of age. These data suggest that various regions of the CNS are functionally compromised in young adult $Fa2h^{-/-}$ mice. The cerebellar deficits in 12-month-old $Fa2h^{flox/flox}$ Cnp1-Cre mice were indistinguishable from $Fa2h^{-/-}$mice, indicating that these phenotypes likely stem from the lack of myelin hFA-galactolipids. In contrast, $Fa2h^{flox/flox}$ Cnp1-Cre mice did not show reduced performance in water maze tasks, indicating that oligodendrocytes are not involved in the learning and memory deficits found in $Fa2h^{-/-}$ mice. These findings provide the first evidence that FA2H has an important function outside of oligodendrocytes in the CNS.

Keywords

fatty acid 2-hydrxylase; oligodendrocytes; leukodystrophy

[*]Correspondence to: Hiroko Hama, Department of Biochemistry and Molecular Biology, Medical University of South Carolina, 173 Ashley Ave., Charleston, SC 29425, USA. Phone: (843) 792-6949; Fax: (843) 792-8568; hama@musc.edu.
[§]Current address: Sanford-Burnham Medical Research Institute, Orlando, Florida

INTRODUCTION

Myelin is a lipid-rich extension of the plasma membrane of oligodendrocytes and Schwann cells that serves to protect the axon from damage as well as increase the nerve conduction rate. Proper neuronal communication requires intact myelin, as many disorders are characterized by damage to and/or loss of myelin, including multiple sclerosis and leukodystrophies. The lipid profile of myelin is quite unique; Galactosylceramide (GalCer) and sulfatide make up approximately 30% of total myelin lipids (Norton and Cammer 1984). More than half of brain GalCer contain 2-hydroxy fatty acids (hFA) as their *N*-acyl chains (hFA-galactolipids) (Bowen and Radin 1968). FA2H is the lipid biosynthetic enzyme responsible for the formation of 2-hydroxy fatty acid, the precursor for hFA-galactolipids (Alderson et al. 2004; Eckhardt et al. 2005).

Recently, three studies reported mutations in the human *FA2H* gene associated with autosomal recessive disorders of the CNS (Dick et al. 2010; Edvardson et al. 2008; Kruer et al. 2010). Edvardson et al. described two mutations that resulted in two distinct clinical outcomes. A mild disorder with spasticity in the lower limbs associated with the D35Y mutation. A severe disorder with progressive leukodystrophy and spastic paraparesis was associated with a point mutation in an intron that resulted in aberrant RNA splicing that excludes exons 5 and 6 from the mRNA (Edvardson et al. 2008). These 2 exons encode the putative catalytic site of FA2H; therefore, the mutated protein is likely devoid of enzymatic activity. In the second study, Dick et al. reported two other mutations (Δ53–58 and R235C) associated with a complicated form of hereditary spastic paraplegia with similar clinical manifestations to the severe form of the disease (Dick et al. 2010). In the most recent study, Kruer et al. reported two mutations (R154C and Y170X) in patients diagnosed with neurodegeneration with brain iron accumulation (NBIA). In all cases, frequent falls and gait disturbances were first noted between age 4 and 11; and progressive spasticity, dystonia, and white matter degeneration followed, except in the patients with D35Y mutation. Currently, the pathogenesis of FA2H deficiency is not fully understood. Given the role of FA2H in myelin hFA-GalCer synthesis, the pathogenesis of FA2H deficiency has been attributed to abnormal myelin lipids.

In the current study, we report CNS phenotypes of a mouse model of FA2H deficiency, in which the mice carry a floxed *Fa2h* allele that, upon Cre-mediated recombination, recapitulated a pathogenic mutation identified in 7 patients (deletion of exons 5 and 6) (Edvardson et al. 2008). Using two different Cre mice, we have developed two versions of *Fa2h* knockout mice. One line of mice has the *Fa2h* deletion in every cell ($Fa2h^{-/-}$ mice, generated by male germline deletion using the 129-Tg(Prm-Cre)58Og/J mice). The other has the deletion in oligodendrocytes and Schwann cells ($Fa2h^{flox/flox}$ Cnp1-Cre), which was generated using mice expressing Cre under the control of the *Cnp1* gene promoter (Lappe-Siefke et al. 2003). $Fa2h^{-/-}$mice showed a number of pathological phenotypes, some of which were previously unrecognized in the CNS, and others manifested in other organ systems. The two versions of *Fa2h* knockout mice allowed us to determine which of these phenotypes stem from myelin lipid abnormalities. We found profound histological and functional changes in the CNS of $Fa2h^{-/-}$mice. Unexpectedly, some of the CNS deficits in $Fa2h^{-/-}$ mice were not present in $Fa2h^{flox/flox}$ Cnp1-Cre mice, indicating that some of the CNS dysfunctions in $Fa2h^{-/-}$ mice are not associated with abnormal oligodendrocytes. Our data suggest that FA2H has other important functions in the CNS in addition to the synthesis of myelin hFA-galactolipids.

MATERIALS AND METHODS

Animals

Mice were maintained in animal care facilities of the Medical University of South Carolina and were treated in accordance with the Institutional Animal Care and Use Committee-approved procedures. They were maintained under 12-hr light:dark cycle and at an ambient temperature of 20–22°C. All mice used in this study are on a mixed 129 and C57BL/6 background.

Conditional *Fa2h* knockout Mice

Three genomic DNA fragments corresponding to the left arm (5 kb), the right arm (3.2 kb), and the targeted region (2 kb) of the mouse *Fa2h* gene were amplified by PCR from a BAC clone containing the *Fa2h* gene [RPCI-22 (129S6/SvEvTac) Mouse BAC Library, Children's Hospital Oakland Research Institute, Oakland, CA]. The fragments were cloned into pVBFRTCKF05 to construct a targeting vector by Vega Biolab (Philadelphia, Pennsylvania, USA) (Fig. 1). Generation of targeted ES cells and chimeric mice were performed by Ozgene (Bentley, Australia). Briefly, linearized targeting vector was electroporated into 129/SvJ embryonic stem cells. G418 resistant ES cell clones were screened for targeted integration by Southern hybridization. The targeted allele ($Fa2h^{tm1Hama}$) is indicated as $Fa2h^{flox}$ in the text. ES cells heterozygous for the targeted allele ($Fa2h^{+/flox}$) were injected into C57BL/6 mouse blastocysts, and resulting male offspring with high coat color chimerism were tested for germline transmission. One-half of the agouti offspring of germline transmitters carried the $Fa2h^{flox}$ allele, as expected. Routine genotyping for the $Fa2h^{flox}$ allele was performed by PCR using tail DNA with primer 1 (ccagtactctggaggctaagg) and primer 2 (ctatatgtgcgtcggtgtttttc) for the $Fa2h^{+}$ allele (218 bp), and with primer 3 (attgaacaagatggattgcac) and 4 (agccatgatggatactttctc) for the $Fa2h^{flox}$ allele (345 bp) (Fig. 1A).

The *Fa2h* null allele ($Fa2h^{tm1.1Hama}$), indicated as $Fa2h^{-}$ in the text, was generated by crossing $Fa2h^{+/flox}$ mice to 129-Tg(Prm-Cre)58Og/J mice (stock #003328, the Jackson Laboratory, Bar Harbor, Maine, USA), in which the Cre recombinase is expressed in male germline cells. The genotype of the offspring was determined using tail DNA and primers 1 and 2 for the $Fa2h^{+}$ allele, and primers 3 and 4 for the $Fa2h^{flox}$ allele. Male $Fa2h^{+/flox}$ Prm-Cre mice were crossed to $Fa2h^{+/+}$ female mice, and the genotype of the offspring was determined by PCR using the tail DNA and primers 1 and 2 for the $Fa2h^{+}$ allele (218 bp), and primers 5 (ctacagtccccattgaaaaac) and 6 (tggtaatactttggttatgctg) for the $Fa2h^{-}$ allele (333 bp) (Fig. 1A, B). The 333-bp PCR product with primers 5 and 6 was sequenced to confirm the expected deletion of the targeted region. The $Fa2h^{+/+}$, $Fa2h^{+/-}$, and $Fa2h^{-/-}$ offspring were born at a ratio of 1:2:1.

Mice with *Fa2h* deleted only in myelin-producing cells were generated using Cnp1-Cre mice, in which the Cre recombinase was expressed in oligodendrocytes and Schwann cells (Lappe-Siefke et al. 2003). $Fa2h^{+/flox}$ Cnp1-Cre mice were crossed to $Fa2h^{flox/flox}$ mice. The genotype of the offspring was determined by PCR using the tail DNA as described above for the $Fa2h^{+}$ and $Fa2h^{flox}$ alleles, and with primers oIMR1084 (gcggtctggcagtaaaaactatc) and oIMR1085 (gtgaaacagcattgctgtcactt) for the Cre transgene. The offspring with the four genotypes ($Fa2h^{+/flox}$ Cnp1-Cre, $Fa2h^{flox/flox}$ Cnp1-Cre, $Fa2h^{+/flox}$, $Fa2h^{flox/flox}$) were born at a ratio of 1:1:1:1. Cre-mediated deletion of the targeted region was confirmed by PCR using brain DNA.

Lipid analysis by thin-layer chromatography

Total lipids were extracted from brain and sciatic nerve as described (Alderson et al. 2006; Scandroglio et al. 2009) with minor modifications. Lipids were extracted with 20 volumes of chloroform/methanol (2:1, v/v). When indicated, lipid extracts were subjected to mild alkaline hydrolysis (in 0.6 M NaOH for 3 hr at 37° C and overnight at room temperature) to remove glycerolipids. Lipid samples were applied on HPTLC plates and developed in chloroform/methanol/water (70:30:4, v/v/v). Lipid spots were visualized under ultraviolet light after spraying with primuline solution (0.005% primuline in acetone/water, 80:20, v/v). Hydroxy and non-hydroxy galactosylceramide standards were purchased from Matreya (Pleasant Gap, Pennsylvania, USA).

Mass spectrometric analyses of lipids

Spinal cord was dissected from 14-month-old *Fa2h*$^{+/-}$ and *Fa2h*$^{-/-}$ males (n=2). Multi-dimensional mass spectrometry-based shotgun lipidomics analyses (Han and Gross 2003; Han and Gross 2005) were performed on a QqQ mass spectrometer (Thermo Fisher TSQ Quantum Ultra, San Jose, California, USA) equipped with an automated nanospray apparatus (Nanomate HD, Advion Bioscience Ltd., Ithaca, New York, USA) and operated with an Xcalibur software system as previously described (Yang et al. 2009).

Brain GalCer from 3-month-old male *Fa2h*$^{+/-}$, *Fa2h*$^{-/-}$, *Fa2h*$^{+/flox}$ Cnp1-Cre, and *Fa2h*$^{flox/flox}$ Cnp1-Cre mice (n=2 for each genotype) were analyzed by LC/MS/MS as previously described (Bielawski et al. 2009).

Histological and immunohistochemical analyses

Brains of male mice (n=2–6 per genotype for each time point) were fixed by immersion in Tellyesniczky/Fekete (Telly's) fixative (Fekete 1938; Lille 1965) overnight at 4°C and stored in 70% ethanol until sectioning. Coronal paraffin sections (5μm) were stained with either hematoxylin/eosin (H&E) to evaluate anatomical structure, or with luxol fast blue (LFB) to evaluate myelin lipids. The blue LFB stain of 2 representative slides per mouse was quantified using CRi Nuance spectral imaging and quantifying system (CRi Inc., Woburn, Massachusetts, USA). Cubed image files were collected at 10 nm wavelength intervals from 500 to 800 nm, with an auto exposure time per wavelength interval at 400x magnification. Both separated and combined QD images were established after determining the QD spectral library and unmixing the cube. We divided the number of pixels represented by the LFB staining by the number of background pixels. We then averaged the number of pixels for each genotype and age, and ran a 2-way ANOVA. Significance was set at $p<0.05$ and Bonferroni post-hoc analyses were run as necessary.

To identify Purkinje neurons, additional slides were stained with anti-calbindin antibodies (1:2000; Swant CB 38, Bellinzona, Switzerland) and visualized using the VECTASTAIN ABC Kit (Vector Laboratories, Burlingame, CA). Amount of staining was quantified using CRi Nuance spectral imaging and quantifying system similar to that described for LFB. Data were analyzed by 2-way ANOVA with significance set at $p<0.05$.

Electrophysiology

Nerve conduction studies were performed on *Fa2h*$^{-/-}$ mice (n=3) and *Fa2h*$^{+/+}$ mice (n=4) at 12 months of age, using a VikingQuest EMG machine (Nicolet instruments, Madison, WI) as previously described (Shy et al. 1997). Mice were anesthetized with ketamine/zylazine by intraperitoneal injection. Body temperature was monitored with a rectal probe connected to an automatic temperature controller (Warner Instrument Corporation), and maintained throughout the testing at 35.5–37° C using a heating lamp. The compound muscle action potential (CMAP) was recorded with a pair of sub-dermal stainless steel

electrodes (Viasys) positioned over the intrinsic foot muscles and proximal interphalangeal joints, respectively. The sciatic nerve (proximal; sciatic notch) or its tibial branch (distal; lateral malleolus) was stimulated sub-dermally using a pair of stainless steel electrodes. A stainless steel, sub-dermal ground electrode was positioned between stimulation and recording sites. The amplitude, latency, and duration of evoked CMAPs were recorded with supramaximal stimulation. The latencies from each site of stimulation, and the distance between the stimulated sites were measured, and the conduction velocities (CV) were calculated (CV= latency from sciatic notch - latency from lateral malleolus/ distance). To document dispersion and/or conduction block, the amplitudes and durations of CMAPs at each site were compared. If the proximally-evoked CMAP has a different waveform and is prolonged, it is considered to be temporally dispersed (Rhee et al. 1990). If the amplitude of the proximally-evoked CMAP is less than one-half of that of the distally-evoked CMAP, it is considered to have conduction block (Rhee et al. 1990).

Electron microscopy

Immediately after the electrophysiology experiments were completed, the mice were transcardially perfused with 0.9% NaCl, followed by 2% glutaraldehyde and 2% paraformaldehye in 0.1 M phosphate buffer (pH 7.4), the optic nerves, cervical spinal cords, and sciatic nerves were dissected and fixed 4 hr at 4°C, then osmicated, dehydrated,and embedded in Epon. Transverse, semithin sections (1 μm) were stained with alkaline toluidine blue and visualized through light microscopy (Leica DMR) using interactive software (Improvision). Thin sections (90 nm thick) were mounted on 2 x 1 mm single-slot, formvar-coated grids, stained with lead citrate and uranyl acetate, and examined with a JOEL 1200 electron microscope. Selected images (on film) were made with a Hitachi 7000 electron microscope, and the negatives were scanned and processed with Photoshop to generate the figures.

General motor activity

Spontaneous locomotor activity (total distance traveled, horizontal activity, and vertical movement-frequency) was assessed in a Digiscan Animal Activity Monitor system (Omnitech Electronics Model RXYZCM(8) TAO, Columbus, Ohio, USA) (Halberda et al. 1997). Data was collected in 5-min intervals for 1 hr and were analyzed by ANOVA as appropriate. Significance was set at $p<0.05$, and Bonferroni post-hoc analyses were conducted as necessary.

Rotarod performance

Motor coordination was evaluated using an accelerating rotarod treadmill (Ugo Basile, Verese, Italy) as described by Boger et al. 2006. The mice were trained to remain on the rotarod for a maximum of 5 min at a set speed of 4 rpm for acclimation to the apparatus on the day before the actual testing. In a typical test, mice were evaluated for 3 consecutive days (trial 1–3). For the time-course experiment (Fig. 5E), mice were acclimated to the apparatus only once for the 2-month time point, and the rest of the testing was performed one trial per time point without re-acclimation. On testing days, mice were tested for their ability to remain on the rotarod at increasing rotation speeds of 4, 8, 16, 24, 32, and 40 rpm. During these tests, the animals were allowed a maximum of 5 min at each rotation speed and a 5-min rest between each rotation speed. The results were averaged to obtain a single value for each genotype at any given rotational speed and/or testing day. Data were analyzed by 3-way ANOVA (Genotype x Trial x Speed) with appropriate post-hoc analyses as necessary. Significance was set at $p<0.05$.

Reversal learning – Water T-maze

Mice were trained to swim to one arm (counterbalanced) of a water T-maze (San Diego Instruments, San Diego, CA, USA) (Del Arco et al. 2007). Mice were divided into squads of 3–4. On training days, subjects were placed, one at a time, into the stem of the maze and allowed to swim to the escape platform. Mice were given 60 sec to locate the platform. Once the platform was located, mice were held on the platform for 3–5 sec before removal from the maze. If the mice did not reach the platform within 60 sec, they were manually guided to the platform and held for 10 sec. After a 2-min rest period, the mouse was again placed in the maze for another trial. All mice were given 4 trials during each daily session. Dependent variables included latency to reach the escape platform and percent correct choices for each 4-trial daily session. Percent correct choices and criterion performance were calculated for each animal following each training session. Criterion performance was set at 75% correct choices (i.e., 3 out of the 4 trials for a given training session) with each swimming attempt being completed in less than 5 sec. Upon meeting this criterion for 3 consecutive days (completed criterion performance), it was recorded that the animal had achieved initial training and the escape platform was reversed (placed in the opposite arm). The training process was repeated as previously described until completed criterion performance was met for the new arm. Data on the graph are shown as number of sessions needed to achieve completed criterion performance for both the initial arm (Initial) and the opposite arm (Reverse); data were analyzed by 2-way ANOVA. Significance was set at $p<0.05$, and Bonferroni post-hoc analyses were run as necessary.

Morris water maze

The Morris maze (Morris et al. 1981) consists of a round tub (60 cm in diameter) that was filled with room-temperature water made opaque with non-fat dry milk. A platform (9.5 cm diameter) was submerged just below the water surface. The tub was enclosed in white walls (100 cm high) with extramaze cues on 3 sides, and the operator served as the cue on the 4th side. There were no obvious intramaze cues. The mouse was placed in the maze starting from one of four predetermined, set locations (labeled North, South, East, or West) and was given 60 sec to locate the hidden platform, which remained in a fixed location (in the Northeast quadrant throughout initial testing and Southwest quadrant during reversal testing). If the mouse did not find the platform in the allotted time, it was gently guided to it. Once the mouse found the platform, the trial was terminated and the mouse was given 15 sec on the platform before being removed from the maze, dried, and placed into the holding cage until the next trial. The mice were given 4 trials per day; the starting location for each trial varied semi-randomly so that starting locations were not given in the same order on consecutive days. The approximate inter-trial interval was 5–8 min, but never less than 5 min. Dependent variables were collected as described for the Water T-maze task. Data on the graph are shown as number of sessions needed to achieve completed criterion performance for both the initial (Initial) and the reverse platform locations (Reverse); data were analyzed by 2-way ANOVA. Significance was set at $p<0.05$, and Bonferroni post-hoc analyses were run as necessary.

RESULTS

Cre-mediated deletion of *Fa2h* in mice

A targeting vector was constructed to contain two loxP sites, one upstream of exon 5 and the other downstream of exon 6, which allows Cre-lox-mediated deletion of the targeted region (Fig. 1A). The loss of these 2 exons was reported in 7 human patients of FA2H deficiency as a result of aberrant RNA processing (Edvardson et al. 2008). The *Fa2h* null allele was generated by a genetic cross between $Fa2h^{+/flox}$ mice and protamine-Cre transgenic mice. When male $Fa2h^{+/flox}$ protamine-Cre mice were crossed with $Fa2h^{+/+}$ females, the $Fa2h^{+/+}$

and *Fa2h*$^{+/-}$ offspring were born at a 1:1 ratio. The *Fa2h*$^{+/-}$ mice were then bred to produce homozygous *Fa2h*$^{-/-}$ mice. The genotypes of offspring were determined by PCR (Fig. 1B). As observed in human patients with the aberrant RNA excluding exon 5 and 6, *Fa2h* mRNA levels were not altered in *Fa2h*$^{-/-}$ mice; *Fa2h*$^{-/-}$ mice expressed a shorter mRNA at the same level as the normal mRNA in control mice in the brain and skin (data not shown). Deletion of exons 5 and 6 in the shorter mRNA in *Fa2h*$^{-/-}$ mice was confirmed by sequencing cDNA prepared from brain RNA (data not shown).

To examine the hFA-galactolipids in the nervous system, we analyzed galactolipids in the brain and sciatic nerve of postnatal day 23 mice by HPTLC. As shown in Fig. 1C, the lower bands corresponding to hFA-GalCer were absent in *Fa2h*$^{-/-}$ mice, and partially replaced by non-hydroxy GalCer (upper bands). Spinal cord lipids from 14-month-old mice were analyzed by mass spectrometry (Fig. 1D). In *Fa2h*$^{-/-}$ mice, hFA-GalCer and hFA-sulfatide were not detectable, while there was no significant difference in non-hydroxy GalCer and a slight decrease in non-hydroxy sulfatide in *Fa2h*$^{-/-}$ mice compared to heterozygous littermates. Consequently, the total galactolipid levels were 40% lower in *Fa2h*$^{-/-}$ mice. Cholesterol, the most abundant myelin lipid, was also 40% lower in *Fa2h*$^{-/-}$ mice compared to heterozygous littermates (Supplementary Table 1). These results are consistent with the significant loss of spinal cord myelin in aged *Fa2h* null mice as reported by Zoller et al. 2008.

Pathological changes of the optic nerve and cervical spinal cord in *Fa2h*$^{-/-}$ mice

We examined semi-thin sections of the left and right optic nerves and cervical spinal cord of 12-month-old *Fa2h*$^{-/-}$ mice (n=4) and *Fa2h*$^{+/+}$ mice (n=4) (Fig. 2 and 3). Each optic nerve and spinal cord from *Fa2h*$^{-/-}$ mice had dozens of abnormal appearing myelinated axons – there were myelin sheaths that surrounded axons with abnormally dense cytoplasm, abnormal accumulations of organelles that could not be resolved by light microscopy, as well as myelin sheaths that did not surround an identifiable axon (indicating that the axon had degenerated). In several optic nerves, we found regions of profound axonal loss; Fig. 2A shows one example. The above pathological findings were enriched in these regions.

We examined the optic nerves by electron microscopy (Fig. 2C). This demonstrated vacuoles, demyelinated axons, myelin sheaths that surrounded axons that had abnormally electron-dense cytoplasm, or accumulations of dense bodies, lysosomes, and mitochondria. The grossly enlarged axons (some more than 20 μm in diameter) usually contained whorls of disorganized neurofilaments as well as dense bodies, lysosomes, and mitochondria; these were sometimes surrounded by an attenuated myelin sheath. These pathological findings were enriched in the large patches where myelinated axons were largely absent. In addition, these regions contained mononuclear cells that did not have the ultrastructural characteristics of oligodendrocytes or astrocytes, and were likely macrophages or microglia (not shown). Only a few apoptotic nuclei were seen, and we could not confidently identify the cell type. Hypertrophied astrocytes were noted, particularly in the subpial region. None of these pathological changes were noted in optic nerves of *Fa2h*$^{+/+}$ mice (Fig. 2D).

In contrast to the optic nerves and the cervical spinal cord, the sciatic nerves of *Fa2h*$^{-/-}$mice contained occasional axons (less than 1% of the total) surrounded by myelin sheaths that were disproportionately thin for the axonal caliber (Fig. 3C), indicating a low level of demyelination followed by remyelination. Consistent with this interpretation, we saw myelin debris in some endoneurial macrophages, and even a few demyelinated axons. None of these features were noted in the sciatic nerves of *Fa2h*$^{+/+}$ mice (Fig. 3D). The myelin sheaths of *Fa2h*$^{-/-}$mice appeared normal – they stained equally well with toluidine blue and had a similar ultrastructure to *Fa2h*$^{+/+}$ mice (Supplementary Figure 1). Consistent with the small

degree of demyelination, the nerve conduction velocities and compound muscle action potentials were not significantly different between *Fa2h*$^{-/-}$ and *Fa2h*$^{+/+}$ mice (Table 1).

Cerebellar dysfunction in *Fa2h*$^{-/-}$ and *Fa2h*$^{flox/flox}$ Cnp1-Cre mice

The majority of the human patients with the severe form of FA2H deficiency experience dystonia and gait disturbance that, at least in part, can be attributed to cerebellar atrophy (Edvardson et al. 2008). We histologically evaluated the brains of both 3-month-old and 12-month-old *Fa2h*$^{-/-}$ and compared them to control mice to assess if our mice showed evidence of cerebellum disruptions. We did not observe any differences in size or gross morphology of the cerebellum of either genotype or age (H&E staining; Fig. 4A). However, luxol fast blue (LFB) staining for myelin lipids revealed decreased staining in the cerebellum of 12-month-old *Fa2h*$^{-/-}$mice compared to control littermates, while there was no difference between these genotypes at 3 months of age (Fig. 4B). Decreased LFB-staining was not observed in the forebrain of 12-month-old *Fa2h*$^{-/-}$ mice. Similar to *Fa2h*$^{-/-}$ mice, *Fa2h*$^{flox/flox}$ Cnp1-Cre mice also had significantly decreased LFB-staining when compared to *Fa2h*$^{+/flox}$ Cnp1-Cre littermates at 12 months of age (Fig. 4C), while there was no significant difference at 6-months of age (not shown). Decreased LFB-staining in the 12-month-old *Fa2h*$^{-/-}$ and *Fa2h*$^{flox/flox}$ Cnp1-Cre mice was confirmed by evaluating the average number of pixels (2-6 mice per genotype at 3, 6, and 12 months of age). Additionally, the immunohistochemical analysis revealed an abnormality in calbindin-positive Purkinje neurons in the older *Fa2h* deficient mice. While the overall number of Purkinje neurons was similar between the mutants and their respective control mice (by pixel counts), older *Fa2h*$^{-/-}$ (Fig. 4D) and *Fa2h*$^{flox/flox}$ Cnp1-Cre mice (Fig. 4E) had many areas of smaller sized or absent Purkinje neurons relative to their respective control mice. Overall, the histological abnormalities in the cerebellum were indistinguishable between *Fa2h*$^{-/-}$ and *Fa2h*$^{flox/flox}$ Cnp1-Cre mice.

The cerebellum contributes to coordination, precision, and accurate timing of movement. Damage to the cerebellum does not cause paralysis, but instead produces disorders in fine movement, equilibrium, posture, and motor learning (Fine et al. 2002). Given the histological disruptions seen in the 12-month-old animals, we evaluated these mice by a series of behavioral tests targeted at movement and balance/coordination. Spontaneous motor activity for male *Fa2h*$^{-/-}$ and control mice is summarized in Fig. 5A. *Fa2h*$^{-/-}$ mice showed significantly reduced ambulation relative to their littermate controls. While all spontaneous locomotion was reduced (both total distance and horizontal activity; $p<0.05$), the greatest difference was seen in the number of vertical movements ($p<0.01$), which requires greater cerebellar involvement. Additionally, *Fa2h*$^{-/-}$ mice showed significantly impaired motor coordination and motor learning relative to normal littermates when assessed using an accelerating rotarod (Fig. 5B). Mice were given a maximum of 5 min at each rotation speed, and data were recorded as the amount of time an animal was able to remain on the bar. ANOVA revealed a significant overall interaction between genotype and rotation speed [$F(10, 144)= 2.03$, $p<0.05$]. Post-hoc analysis revealed that *Fa2h*$^{-/-}$ mice had significantly impaired performance (relative to controls) at all speeds greater than 4 rpm. Importantly, the behavioral performance of *Fa2h*$^{-/-}$ mice was nearly identical to performance by *Fa2h*$^{flox/flox}$ Cnp1-Cre mice at 12 months of age; *Fa2h*$^{flox/flox}$ Cnp1-Cre mice had reduced ambulation, especially vertical activity (Fig. 5C), and significantly impaired rotarod performance compared to *Fa2h*$^{+/flox}$ Cnp1-Cre littermates [Fig. 5D; $F(10, 144)= 2.03$, $p>0.05$]. With respect to rotarod performance, both groups of control mice were able to improve their performance over the successive trials. In contrast, *Fa2h*$^{-/-}$and *Fa2h*$^{flox/flox}$ Cnp1-Cre mice showed no improvement over the 3 trials, which implicates the *Fa2h* deletion in oligodendrocytes as detrimental to motor learning. Impaired performance was also observed with 12-month-old female *Fa2h*$^{-/-}$ mice (Supplementary Fig. 2). These

findings, combined with the spontaneous locomotion deficits and altered cerebellar architecture (Fig. 4), further suggests the necessity of hFA-galactolipids in maintaining normal motor coordination and motor learning behavior.

As mentioned above, we did not see any histological abnormalities in 3-month-old *Fa2h*$^{-/-}$ mice (Fig. 4), nor did these mice display any deficiencies in general locomotion and rotarod performance (Supplementary Fig. 3A and B). Furthermore, *Fa2h*$^{+/flox}$ Cnp1-Cre mice were not significantly different than control mice at 6 months of age (Supplementary Fig. 3C and D). To determine when the effects of the *Fa2h* mutation began to disrupt behavior, a separate group of animals was evaluated monthly via rotarod performance (Fig. 5E). As expected, *Fa2h*$^{-/-}$mice did not differ from control mice at months 2–6; however, differences between the genotypes emerged at the 7-month time point. Only control mice began improving their performance (motor learning) at months 7 and 8, while *Fa2h*$^{-/-}$ mice began showing significantly deteriorated performance. It was evident during the 9-month testing session that *Fa2h*$^{-/-}$ mice were exhibiting significantly deteriorated performance as they had a significantly impaired ability to remain on the bar at all speeds above 8 rpm ($p<0.05$), which was comparable to the 12-month-old *Fa2h*$^{-/-}$ mice from the previous figure ($p>0.05$).

Learning and memory are impaired in *Fa2h*$^{-/-}$ mice but not in *Fa2h*$^{flox/flox}$ Cnp1-Cre mice

In all reported cases of human FA2H deficiency, onset of the disease is 4–11 years of age, and many of the patients are described as exhibiting mild to moderate cognitive decline following seemingly normal early development. Thus, we were interested in defining the earliest signs of CNS deficits in *Fa2h*$^{-/-}$ mice. Although the difference in rotarod performance was clear at 7 months of age (Fig. 5E), the question remained whether subtle CNS abnormalities existed earlier, particularly with regard to cognitive ability. Animals were tested in a water T-maze for their ability to find an escape platform located in one of the two arms (initial learning), and were subsequently tested for their ability to locate the platform that was repositioned in the opposite arm from their initial training (reversal learning). The water T-maze task serves as a simple memory assay given that animals are not forced to rely on one set of environmental cues (e.g., spatial cues, directional cues, etc.), but can provide insight into memory formation and reversal learning processes with relatively little training. Fig. 6A illustrates that while all mice performed similarly during initial learning [$F(15,1)=0.063$, $p=0.85$], *Fa2h*$^{+/+}$ mice had significantly better reversal learning performance than *Fa2h*$^{-/-}$ mice [$F(15,1)=5.063$, $p=0.02$].

Given the striking difference in water T-maze performance, we next evaluated spatial learning/memory using a Morris water maze, measuring both initial and reversal learning (Fig. 6B). While similar in concept to the water T-maze, the Morris water maze is a more challenging task that specifically evaluates an animal's ability to utilize spatial cues. We determined that younger (< 6 months) *Fa2h*$^{-/-}$ animals do not display impaired vision and are indistinguishable from *Fa2h*$^{+/+}$ mice on vision performance tasks (data not shown). Similarly to the water T maze task, *Fa2h*$^{-/-}$ mice had significantly impaired reversal learning performance than *Fa2h*$^{+/+}$ mice In the Morris water maze task [$F(13,1)=10.658$, $p=0.01$]. Interestingly, they also showed impaired initial learning [$F(13,1)=7.725$, $p=0.02$], indicating a severe memory deficit. Although gross histological analyses (H&E and LFB staining) did not reveal differences in the hippocampus (essential for spatial learning) between *Fa2h*$^{+/+}$ and *Fa2h*$^{-/-}$ mice, these behavioral data indicate that FA2H is essential for proper CNS functioning. Surprisingly, when we evaluated the behavioral performance in *Fa2h*$^{flox/flox}$ Cnp1-Cre mice and *Fa2h*$^{+/flox}$ Cnp1-Cre mice, there was no difference in behavior between the two groups on either the water T-maze [Fig. 6C; Initial: $F(16,1)=1.692$, $p=0.21$; Reverse: $F(16,1)=1.363$, $p=0.26$] or Morris water maze tasks [Fig. 6D; Initial: $F(16,1)=0.002$, $p=0.96$; Reverse: $F(16,1)=0.926$, $p=0.35$]. Because the results with *Fa2h*$^{flox/flox}$ Cnp1-Cre mice were unexpected, a second tail biopsy was taken from all

experimental mice upon conclusion of the behavioral studies, and their genotypes were confirmed. In the initial report of Cnp1-Cre mice, Lappe-Siefke et al. used a lacZ reporter gene to show that Cre was specifically expressed by oligodendrocytes in white matter tracts in the brain (Lappe-Siefke et al. 2003). Nevertheless, there was a concern about incomplete *Fa2h* deletion in our mice, resulting in a small population of oligodendrocytes producing enough myelin hFA-galactolipids to obscure the phenotype. This possibility was eliminated by myelin lipid analyses. The absence of hFA-GalCer was evident in $Fa2h^{flox/flox}$ Cnp1-Cre mice at 10 weeks of age based on the thin-layer chromatogram of brain lipids (Fig. 6E). Detailed galactolipid measurements by mass spectrometry showed a total loss of brain hFA-galactolipids in 3-month-old $Fa2h^{-/-}$ and $Fa2h^{flox/flox}$ Cnp1-Cre mice (Fig. 6F, Supplementary Table 2). These data indicate that the learning/memory deficits in $Fa2h^{-/-}$ mice were not caused by the loss of myelin hFA-galactolipids but by deficiencies in other aspects of the CNS.

DISCUSSION

In the present study we created a floxed *Fa2h* allele and developed two versions of *Fa2h* knockout mice; one with *Fa2h* deleted in all cells ($Fa2h^{-/-}$ mice), and the other with *Fa2h* deleted in oligodendrocytes and Schwann cells ($Fa2h^{flox/flox}$ Cnp1-Cre mice). The two models allowed us to assess oligodendrocyte-derived and non-oligodendrocyte-derived CNS phenotypes of $Fa2h^{-/-}$mice. The mutation we have generated, a genomic deletion encompassing exons 5 and 6, recapitulated one of the mutations found in human FA2H deficiency, though the deletion in the patients occurred during RNA splicing due to a point mutation in an intron.

The axonal degeneration seen in the optic nerve and spinal cord of the $Fa2h^{-/-}$ mice is similar to what was described by Zoller et al. 2008. They did not, however, note regions of profound axonal loss or abnormally enlarged axons. The pathological changes we observed are similar to those reported in the adult-onset CNS demyelination mouse models, in which oligodendrocyte cell death was genetically induced (Pohl et al. 2011; Traka et al. 2010). We suspect that the abnormally enlarged axons are, in effect, transected (Lampert 1967), as occurs in demyelinating lesions of multiple sclerosis (Trapp et al. 1998).

We found evidence of a low level of demyelination and remyelination in the peripheral nerves of 12-month-old $Fa2h^{-/-}$ mice. That the sciatic nerves appear mostly normal is consistent with their normal nerve conduction velocities. Our histological findings, however, differ from those reported by Zoller et al. (2008). They found diminished staining with toluidine blue and splitting of myelin lamellae. It seems unlikely that the global deletion of *Fa2h* resulted in a “myelin phenotype” that was not found in our mice. Technical issues in processing the tissue are a possible explanation.

In characterizing the neuropathological phenotype of our *Fa2h* knockout mice, we were particularly interested in identifying similarities to the human disease phenotype. As seen in human patients, early development appeared normal in $Fa2h^{-/-}$ mice, which was also reported by Zoller et al. 2008. No pathological phenotype was previously identified in young adult $Fa2h^{-/-}$mice. We first focused on uncovering possible cerebellar deficits in our $Fa2h^{-/-}$ mice because in all cases of human FA2H deficiency reported to date, the affected children presented with initial signs of gait abnormality and frequent falls between age 4 and 11, which is consistent with cerebellar abnormality (Dick et al. 2008; Dick et al. 2010; Edvardson et al. 2008; Kruer et al. 2010). As the disease progressed, many of the patients showed additional signs of cerebellar involvement and cerebellar atrophy. Histological and behavioral analyses of our mutant mice revealed that abnormal cerebellar histology and significantly disrupted motor function in both $Fa2h^{-/-}$ and $Fa2h^{flox/flox}$ Cnp1-Cre mice at 12

months of age. A time-course study showed that significantly impaired motor coordination was detectable in *Fa2h*$^{-/-}$ mice at 7 months and older with no signs of motor learning, suggesting the disruption of cerebellum had begun earlier than 7 months of age. Thus, CNS pathology of *Fa2h*$^{-/-}$ mice is not limited to aged animals. Importantly, the cerebellar deficits were indistinguishable between *Fa2h*$^{-/-}$ and *Fa2h*$^{flox/flox}$ Cnp1-Cre mice, suggesting that the cerebellar phenotypes stem from the loss of myelin hFA-galactolipids, causing demyelination and subsequent axonal loss. The precise mechanism of the reduced myelin stability in *Fa2h*$^{-/-}$ mice is currently unknown. Given the strong preference of UDP-galactose:ceramide galactosyltransferase (the enzyme that synthesizes GalCer) for hFA-ceramide over non-hydroxy ceramide (Schaeren-Wiemers et al. 1995), an imbalance between GalCer synthesis and turnover may occur in the absence of hFA in such a way that the normal rate of GalCer degradation is not matched by the rate of replenishing, leading to gradual self-destruction of myelin.

Our study also revealed significantly impaired spatial learning and memory in *Fa2h*$^{-/-}$mice at 4 months of age. Surprisingly, the deficits in learning and memory were not present in *Fa2h*$^{flox/flox}$ Cnp1-Cre mice. As in *Fa2h*$^{-/-}$ mice, hFA-galactolipids were completely absent in *Fa2h*$^{flox/flox}$ Cnp1-Cre mice, indicating that this phenotype is not associated with hFA-galactolipids. Previous studies showed *Fa2h* expression in oligodendrocytes by *in situ* hybridization (Eckhardt et al. 2005) and by immunoblot (Alderson et al. 2006). More recent gene expression profiling studies also showed *Fa2h* expression in oligodendrocytes (Golan et al. 2008; Howng et al. 2010; Stritt et al. 2009). Nonetheless, our finding that the learning and memory deficits are present only in *Fa2h*$^{-/-}$ mice and not in *Fa2h*$^{flox/flox}$ Cnp1-Cre mice could not be explained by the loss of FA2H function in oligodendrocytes. Rather, our finding provides the first evidence for a non-myelin-associated function of FA2H in the CNS.

The task in a Morris water maze test involves recognizing and remembering visual cues to locate a hidden platform, which requires intact hippocampus (Morris et al. 1982). Hence, FA2H may have a role in proper development and neural connectivity in the hippocampus. Preliminary histological analysis revealed no gross abnormality in the hippocampus of *Fa2h*$^{-/-}$mice. Further studies for detailed cellular organization are needed to determine the cause of this phenotype. It is also possible that FA2H is involved in cell signaling that determines neural connectivity in the hippocampus. It is of interest to note that cultured rat cortical neurons showed robust, but transient, upregulation of *Fa2h* expression during differentiation (our unpublished data). We previously showed that FA2H modulates the cAMP signaling pathway in Schwannoma cells (Alderson and Hama 2009). It is conceivable that an FA2H-dependent regulatory mechanism for cAMP signaling exists in differentiating neurons. Further investigation is warranted to determine the role of FA2H in the hippocampus.

In conclusion, a deletion of exons 5 and 6 in the mouse *Fa2h* gene causes a disease of the CNS that shares some aspect of the clinical manifestations of human FA2H deficiency. In addition, some of the CNS abnormalities are not associated with deficiencies in oligodendrocytes and myelin. Further investigation of our *Fa2h* knockout mice will likely provide novel insight into the disease mechanism of FA2H deficiency. Unlike other leukodystrophies, this disease is caused by a lack of lipids. As such, there is a distinct possibility that it could be treatable by replacing the missing lipids. The early signs of the neurological abnormalities of *Fa2h*$^{-/-}$ mice identified in this study could be used in establishing a sensitive functional assay for *in vivo* efficacy of potential lipid therapeutics.

Supplementary Material

Refer to Web version on PubMed Central for supplementary material.

Acknowledgments

We thank Dr. Klaus-Amin Nave for providing Cnp1-Cre mice; Drs. Ann-Charlotte Granholm and Maurizio Del Poeta for sharing their equipment; Dr. Brian Popko for helpful discussions; Margaret Romano, Justin Snider, and Dr. Xi-tian Xu for technical assistance. This work was supported by NIH Grants NS056075 (to HH), NS060807 (to HH), AG31675 (to XH), NS43174 (to SSS), RR017677, and RR16434. This work was conducted in a facility constructed with support from NIH Grant C06 RR015455.

References

Alderson NL, Hama H. Fatty acid 2-hydroxylase regulates cAMP-induced cell cycle exit in D6P2T Schwannoma cells. J Lipid Res. 2009; 50:1203–8. [PubMed: 19171550]

Alderson NL, Maldonado EN, Kern MJ, Bhat NR, Hama H. FA2H-dependent fatty acid 2-hydroxylation in postnatal mouse brain. J Lipid Res. 2006; 47:2772–80. [PubMed: 16998236]

Alderson NL, Rembiesa BM, Walla MD, Bielawska A, Bielawski J, Hama H. The human FA2H gene encodes a fatty acid 2-hydroxylase. J Biol Chem. 2004; 279:48562–8. [PubMed: 15337768]

Bielawski J, Pierce JS, Snider J, Rembiesa B, Szulc ZM, Bielawska A. Comprehensive quantitative analysis of bioactive sphingolipids by high-performance liquid chromatography-tandem mass spectrometry. Methods Mol Biol. 2009; 579:443–67. [PubMed: 19763489]

Boger HA, Middaugh LD, Huang P, Zaman V, Smith AC, Hoffer BJ, Tomac AC, Granholm AC. A partial GDNF depletion leads to earlier age-related deterioration of motor function and tyrosine hydroxylase expression in the substantia nigra. Exp Neurol. 2006; 202:336–47. [PubMed: 16889771]

Bowen DM, Radin NS. Hydroxy fatty acid metabolism in brain. Adv Lipid Res. 1968; 6:255–72. [PubMed: 4180000]

Del Arco A, Segovia G, Garrido P, de Blas M, Mora F. Stress, prefrontal cortex and environmental enrichment: studies on dopamine and acetylcholine release and working memory performance in rats. Behav Brain Res. 2007; 176:267–73. [PubMed: 17097747]

Dick KJ, Al-Mjeni R, Baskir W, Koul R, Simpson MA, Patton MA, Raeburn S, Crosby AH. A novel locus for an autosomal recessive hereditary spastic paraplegia (SPG35) maps to 16q21-q23. Neurology. 2008; 71:248–52. [PubMed: 18463364]

Dick KJ, Eckhardt M, Paisán-Ruiz C, Alshehhi AA, Proukakis C, Sibtain NA, Maier H, Sharifi R, Patton MA, Bashir W, et al. Mutation of FA2H underlies a complicated form of hereditary spastic paraplegia (SPG35). Hum Mutat. 2010; 31:E1251–E1260. [PubMed: 20104589]

Eckhardt M, Yaghootfam A, Fewou SN, Zoller I, Gieselmann V. A mammalian fatty acid hydroxylase responsible for the formation of alpha-hydroxylated galactosylceramide in myelin. Biochem J. 2005; 388:245–54. [PubMed: 15658937]

Edvardson S, Hama H, Shaag A, Gomori JM, Berger I, Soffer D, Korman SH, Taustein I, Saada A, Elpeleg O. Mutations in the fatty acid 2-hydroxylase gene are associated with leukodystrophy with spastic paraparesis and dystonia. Am J Hum Genet. 2008; 83:643–8. [PubMed: 19068277]

Fekete E. A comparative morphological study of the mammary gland in a high and a low tumor strain of mice. Am J Pathol. 1938; 14:557–578.5. [PubMed: 19970409]

Fine EJ, Ionita CC, Lohr L. The history of the development of the cerebellar examination. Semin Neurol. 2002; 22:375–84. [PubMed: 12539058]

Golan N, Adamsky K, Kartvelishvily E, Brockschnieder D, Mobius W, Spiegel I, Roth AD, Thomson CE, Rechavi G, Peles E. Identification of Tmem10/Opalin as an oligodendrocyte enriched gene using expression profiling combined with genetic cell ablation. Glia. 2008; 56:1176–86. [PubMed: 18571792]

Halberda JP, Middaugh LD, Gard BE, Jackson BP. DAD1- and DAD2-like agonist effects on motor activity of C57 mice: differences compared to rats. Synapse. 1997; 26:81–92. [PubMed: 9097408]

Han X, Gross RW. Global analyses of cellular lipidomes directly from crude extracts of biological samples by ESI mass spectrometry: a bridge to lipidomics. J Lipid Res. 2003; 44:1071–9. [PubMed: 12671038]

Han X, Gross RW. Shotgun lipidomics: electrospray ionization mass spectrometric analysis and quantitation of cellular lipidomes directly from crude extracts of biological samples. Mass Spectrom Rev. 2005; 24:367–412. [PubMed: 15389848]

Howng SY, Avila RL, Emery B, Traka M, Lin W, Watkins T, Cook S, Bronson R, Davisson M, Barres BA, et al. ZFP191 is required by oligodendrocytes for CNS myelination. Genes Dev. 2010; 24:301–11. [PubMed: 20080941]

Kruer MC, Paisan-Ruiz C, Boddaert N, Yoon MY, Hama H, Gregory A, Malandrini A, Woltjer RL, Munnich A, Polster BJ, et al. Defective FA2H leads to a novel form of neurodegeneration with brain iron accumulation (NBIA). Ann Neurol. 2010; 68:611–8. [PubMed: 20853438]

Lampert PW. A comparative electron microscopic study of reactive, degenerating, regenerating, and dystrophic axons. J Neuropathol Exp Neurol. 1967; 26:345–68. [PubMed: 5229871]

Lappe-Siefke C, Goebbels S, Gravel M, Nicksch E, Lee J, Braun PE, Griffiths IR, Nave KA. Disruption of Cnp1 uncouples oligodendroglial functions in axonal support and myelination. Nat Genet. 2003; 33:366–74. [PubMed: 12590258]

Lille, RD. Histopathologic Technique and Practical Histochemistry. New York, NY: McGraw-Hill; 1965.

Morris B, Morris R, Kenyon CJ. Effect of adrenalectomy on the transmission of IgG in young rats. Biol Neonate. 1981; 39:239–45. [PubMed: 7260208]

Morris RG, Garrud P, Rawlins JN, O'Keefe J. Place navigation impaired in rats with hippocampal lesions. Nature. 1982; 297:681–3. [PubMed: 7088155]

Norton, WT.; Cammer, W. Isolation and characterization of myelin. In: Morell, P., editor. Myelin. New York: Plenum; 1984. p. 147-195.

Pohl HBF, Porcheri C, Mueggler T, Bachmann LC, Martino G, Riethmacher D, Franklin RJM, Rudin M, Suter U. Genetically Induced Adult Oligodendrocyte Cell Death Is Associated with Poor Myelin Clearance, Reduced Remyelination, and Axonal Damage. J Neurosci. 2011; 31:1069–1080. [PubMed: 21248132]

Rhee EK, England JD, Sumner AJ. A computer simulation of conduction block: effects produced by actual block versus interphase cancellation. Ann Neurol. 1990; 28:146–56. [PubMed: 2221844]

Scandroglio F, Loberto N, Valsecchi M, Chigorno V, Prinetti A, Sonnino S. Thin layer chromatography of gangliosides. Glycoconj J. 2009; 26:961–73. [PubMed: 18704684]

Schaeren-Wiemers N, van der Bijl P, Schwab ME. The UDP-galactose:ceramide galactosyltransferase: expression pattern in oligodendrocytes and Schwann cells during myelination and substrate preference for hydroxyceramide. J Neurochem. 1995; 65:2267–78. [PubMed: 7595516]

Shy ME, Arroyo E, Sladky J, Menichella D, Jiang H, Xu W, Kamholz J, Scherer SS. Heterozygous P0 knockout mice develop a peripheral neuropathy that resembles chronic inflammatory demyelinating polyneuropathy (CIDP). J Neuropathol Exp Neurol. 1997; 56:811–21. [PubMed: 9210878]

Stritt C, Stern S, Harting K, Manke T, Sinske D, Schwarz H, Vingron M, Nordheim A, Knoll B. Paracrine control of oligodendrocyte differentiation by SRF-directed neuronal gene expression. Nat Neurosci. 2009; 12:418–27. [PubMed: 19270689]

Traka M, Arasi K, Avila RL, Podojil JR, Christakos A, Miller SD, Soliven B, Popko B. A genetic mouse model of adult-onset, pervasive central nervous system demyelination with robust remyelination. Brain. 2010; 133:3017–29. [PubMed: 20851998]

Trapp BD, Peterson J, Ransohoff RM, Rudick R, Mork S, Bo L. Axonal transection in the lesions of multiple sclerosis. N Engl J Med. 1998; 338:278–85. [PubMed: 9445407]

Yang K, Cheng H, Gross RW, Han X. Automated lipid identification and quantification by multidimensional mass spectrometry-based shotgun lipidomics. Anal Chem. 2009; 81:4356–68. [PubMed: 19408941]

Zoller I, Meixner M, Hartmann D, Bussow H, Meyer R, Gieselmann V, Eckhardt M. Absence of 2-hydroxylated sphingolipids is compatible with normal neural development but causes late-onset axon and myelin sheath degeneration. J Neurosci. 2008; 28:9741–54. [PubMed: 18815260]

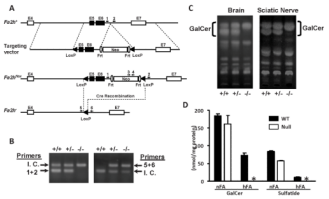

Fig. 1. Deletion of exons 5 and 6 of *Fa2h* eliminates hFA-galactolipids in the nervous system

(A) The targeting vector and the $Fa2h^{flox}$ and $Fa2h^{-}$ alleles. Exons 5 and 6 (E5, E6) of the $Fa2h^{flox}$ allele were successfully excised *in vivo* by Cre recombinase. Note that the diagram is not to scale. (B) PCR-genotyping. The agarose gel on the left shows the presence or absence of the $Fa2h^{+}$ allele amplified by primers 1 and 2. The agarose gel on the right shows the presence or absence of the $Fa2h^{-}$ allele amplified by primers 5 and 6. I.C., internal control. (C) HPTLC analysis of myelin galactosylceramide. Alkaline-resistant lipids were analyzed by HPTLC. Lipids were extracted from brain (2 mg protein equivalent per lane) and sciatic nerve (100 mg protein equivalent per lane) from 23-day-old males. GalCer, galactosylceramide. (D) Analysis of spinal cord lipids by mass spectrometry. Total lipids were extracted from spinal cord tissue of 14-month-old male $Fa2h^{+/-}$ mice (WT, n=2, black bars) and $Fa2h^{-/-}$ mice (Null, n=2, white bars). Asterisks (*) denote below detectable levels. The data shown are the combined levels of the four groups of galactolipids [non-hydroxy (nFA) and hydroxy (hFA) galactosylceramide and sulfatide], each including various molecular species with different *N*-acyl chains. The values for individual molecular species are shown in Supplementary Table 1.

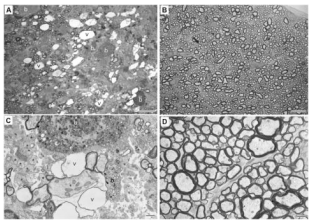

Fig. 2. Pathological findings in the optic nerves of *Fa2h*-null mice

Images from semi-thin (A, B) and thin (C, D) sections of optic nerves from 12-month-old $Fa2h^{-/-}$ (A, C) and $Fa2h^{+/+}$ (B, D) mice are shown. (A) A region of a nerve with markedly reduced numbers of myelinated axons as well as many vacuoles (v) and enlarged bulbous axons (b). (B) A similar region of a normal nerve. Note the dense packing of myelinated axons that range from 0.5 to 3 microns in diameter. (C) An electron micrograph of a similarly affected region as in (A), showing the fine structure of vacuoles (v), demyelinated axons (asterisks), and two bulbous axons (b) that are filled with dense bodies, lysosomes, and mitochondria. (D) An electron micrograph of a similar region of a normal nerve. Scale bar: 10 μm in panels A and B, 1 μm in panels B and D.

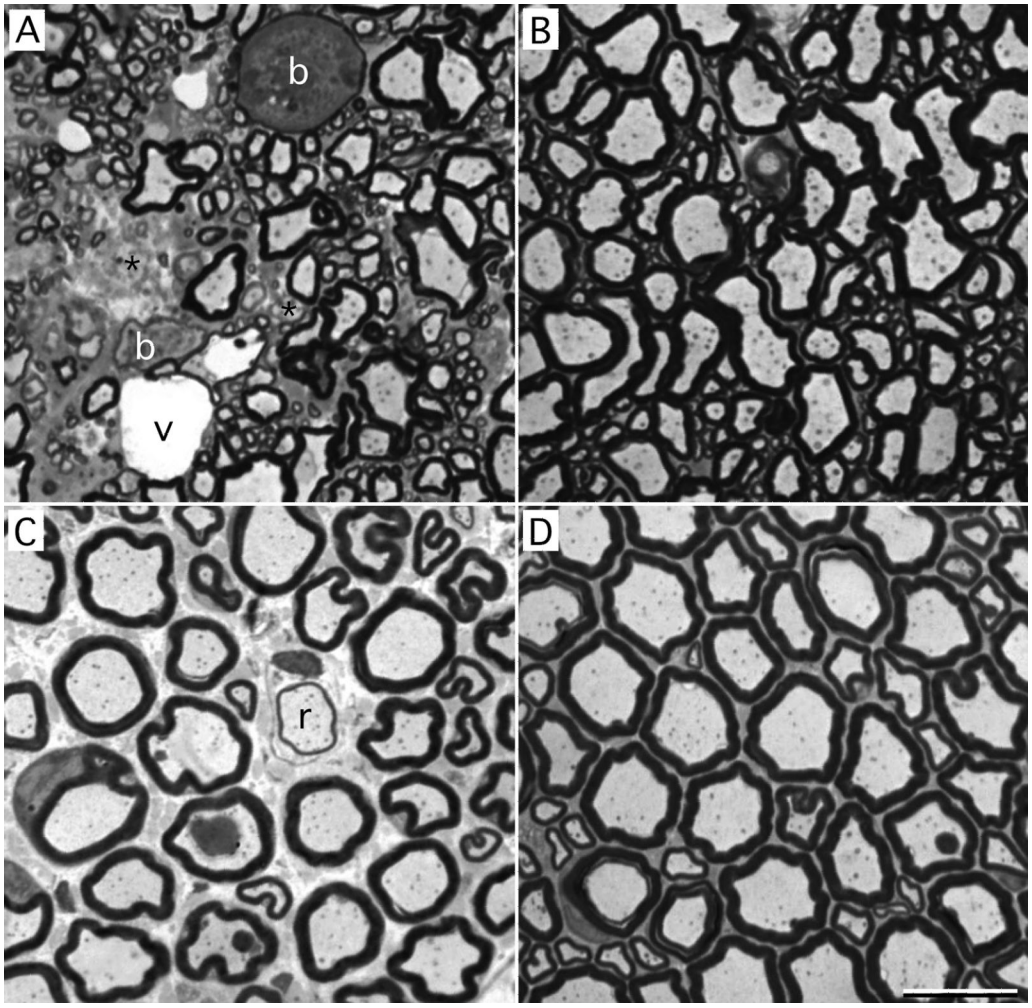

Fig. 3. Pathological findings in the *Fa2h*-null mice

These are images of semi-thin sections of the ventral funiculus of the cervical spinal cord (A, B) and tibial nerves (C, D) from 12 month old $Fa2h^{-/-}$ mice (A, C) or $Fa2h^{+/+}$ mice (B, D). The spinal cord of the $Fa2h^{-/-}$ mice contains demyelinated axons (asterisks), as well as vacuoles (v) and enlarged bulbous axons (b) filled with dense bodies, lysosomes, and mitochondria (not visible at this magnification). The sciatic nerve of the $Fa2h^{-/-}$ mice has a few remyelinated axons (r). Scale bars: 10 μm.

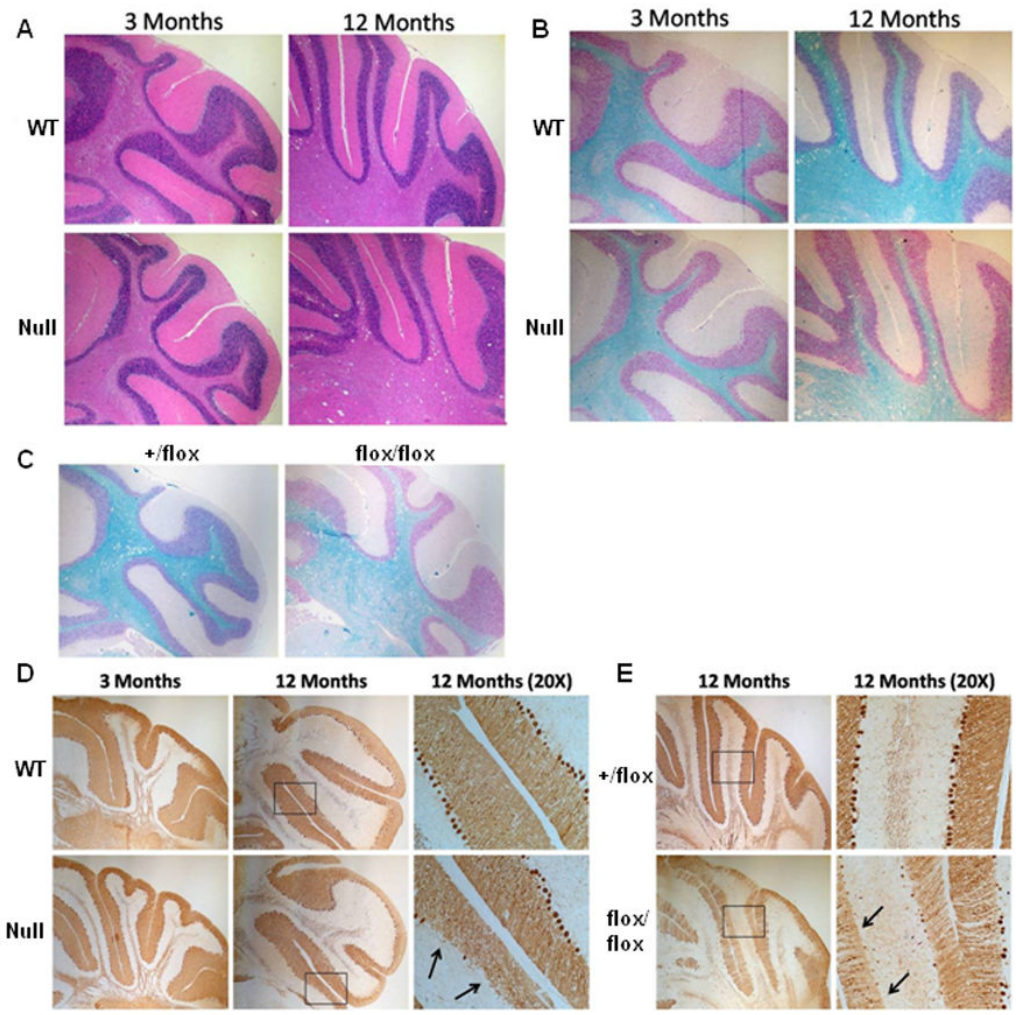

Fig. 4. Cerebellum histology

(A) Overall cerebellum histology (size and gross morphology) of 3- or 12-month-old male *Fa2h*$^{-/-}$ (Null) and control mice (WT) did not differ from one another (H&E, 4x magnification). (B) LFB staining of the cerebellum. While 3-month-old *Fa2h*$^{-/-}$ and control mice were identical, 12-month-old *Fa2h*$^{-/-}$ mice exhibited significantly reduced staining relative to control littermates (4x magnification). (C) LFB staining of 12-month-old *Fa2h*$^{+/flox}$ Cnp1-Cre (+/flox) and *Fa2h*$^{flox/flox}$ Cnp1-Cre (flox/flox) littermates (4x magnification). (D) Calbindin immunostaining of the cerebellum. *Fa2h*$^{-/-}$ mice have altered size and distribution of Purkinje neurons relative to control mice as evidenced by an irregular pattern of calbindin-immunoreactive Purkinje neurons (denoted by black arrows). Left and center panels, 4x magnification; right panels, 20x magnification of the black rectangles in center panels. (E) Calbindin immunostaining of the cerebellum of *Fa2h*$^{+/flox}$ Cnp1-Cre (+/flox) and *Fa2h*$^{flox/flox}$ Cnp1-Cre mice (flox/flox). The black arrows denote areas with disrupted Purkinje neurons. Left panels, 4x magnification; right panels, 20x magnification of the black rectangles in left panels.

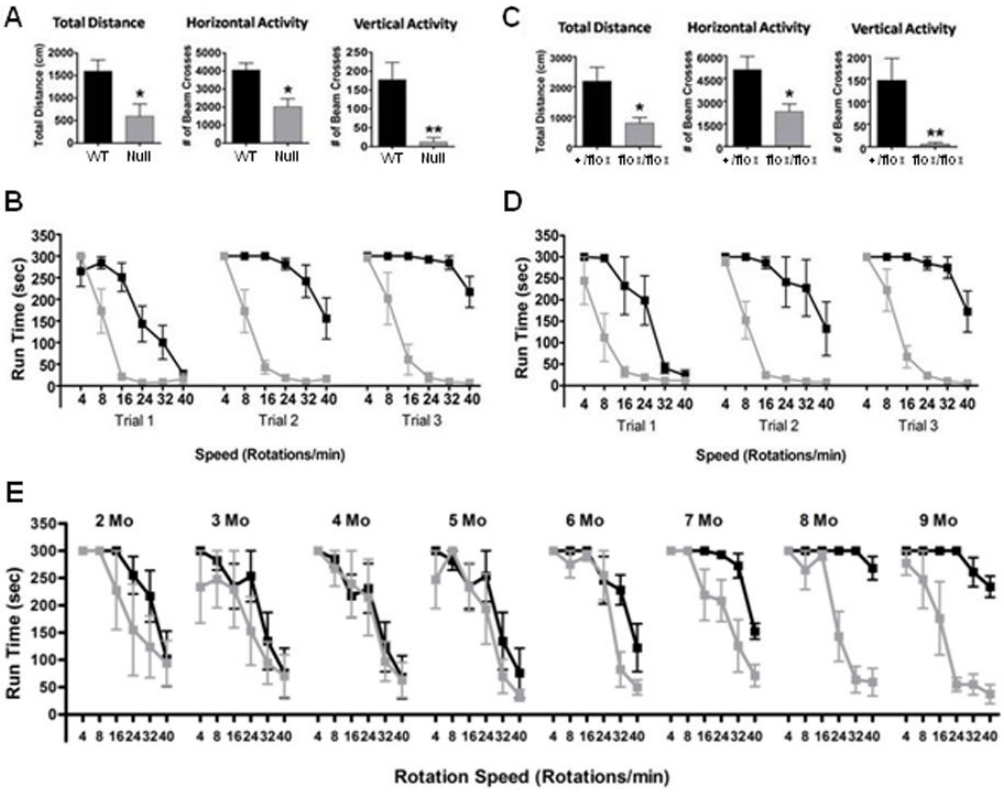

Fig. 5. Behavioral analyses reveal motor deficits in *Fa2h* deficient mice

(A) General motor activity of 12-month-old male *Fa2h*$^{-/-}$ mice (Null, n=5, grey bars) and their littermate controls (WT, n=5, black bars). The control littermates included *Fa2h*$^{+/+}$ and *Fa2h*$^{+/-}$ mice, whose performances were indistinguishable from one another (p>0.05). *, p<0.05; **, p<0.01. (B) Motor coordination and motor learning assessed using an accelerating rotarod device. Grey squares/lines, *Fa2h*$^{-/-}$ mice (n=5); black squares/lines, control littermates (n=5). (C&D) Motor deficits in 12-month-old *Fa2h*$^{flox/flox}$ Cnp1-Cre mice (flox/flox, n=7, grey bars/ squares/lines) were practically identical to *Fa2h*$^{-/-}$ mice. They showed reduced general ambulation (panel C; *, p<0.05; **, p<0.01) and impaired rotarod performance (panel D, p<0.05) in comparison to *Fa2h*$^{+/flox}$ Cnp1-Cre mice (+/flox, n=5, black bars/squares/lines) at all speeds greater than 4 rpm. All data are presented as mean±standard error. (E) Motor deficits emerge at 7 months of age. A separate group of male *Fa2h*$^{-/-}$ mice (n=4, grey squares/lines) and control mice (n=6, black squares/lines) were tested monthly for rotarod performance. The control group included age-matched *Fa2h*$^{+/+}$ and *Fa2h*$^{+/-}$ mice, whose performances were indistinguishable from one another (p>0.05). All data are presented as mean±standard error.

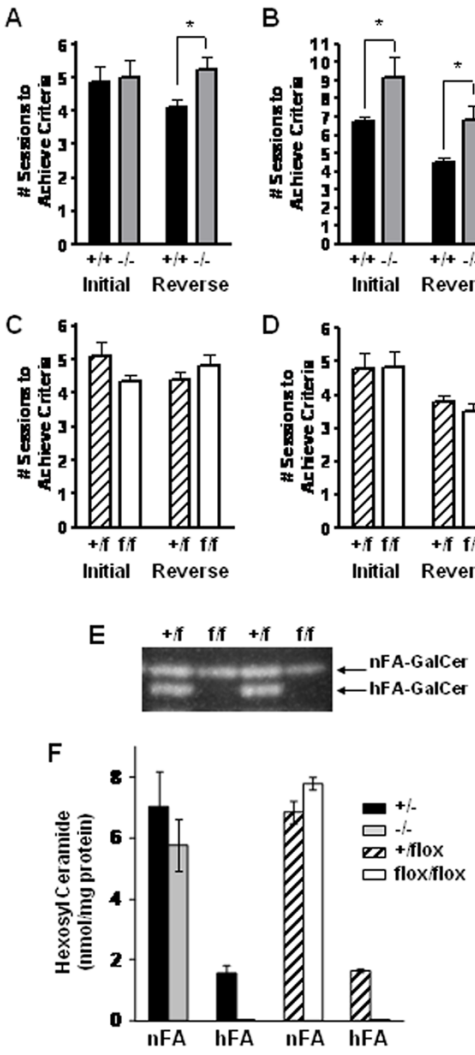

Fig. 6. Learning and memory deficits are present in *Fa2h*$^{-/-}$ mice but not in *Fa2h*$^{flox/flox}$ Cnp1-Cre mice

(A) 3-month-old male *Fa2h*$^{+/+}$ mice [black bars (+/+), n=8] and *Fa2h*$^{-/-}$ mice [grey bars (−/−), n=8] were evaluated for their performance on a water T-maze task. No differences were seen between the genotypes on their ability to locate and swim to a hidden platform (Initial, $p>0.05$). After initial training, the platform was placed in the opposite arm. *Fa2h*$^{+/+}$ mice took significantly fewer sessions to learn the new platform location (Reverse; *, $p< 0.015$) than *Fa2h*$^{-/-}$ mice. All data are presented as mean+standard error. (B) A separate group of 4-month-old *Fa2h*$^{+/+}$ mice [black bars (+/+), n=8] and *Fa2h*$^{-/-}$ mice [grey bars (−/−), n=5] were trained to swim to a hidden platform within a Morris water maze. *Fa2h*$^{-/-}$ mice took significantly more sessions to learn the location of the platform compared to *Fa2h*$^{+/+}$ mice, (Initial; *, $p<0.05$). Once learning was achieved, the platform was moved to a new location and training was repeated. Again, *Fa2h*$^{-/-}$ mice took significantly more sessions to learn the new location of the platform (Reverse; *, $p<0.05$). (C) Water T-maze test was performed with male *Fa2h*$^{+/flox}$ Cnp1-Cre mice [hatched bars (+/f), n=10] and *Fa2h*$^{flox/flox}$ Cnp1-Cre mice [white bars (f/f), n=6]. No significant difference was observed between the two groups for both Initial ($p>0.05$) and Reverse ($p>0.05$). (D) Morris water maze test was performed with male *Fa2h*$^{+/flox}$ Cnp1-Cre mice [hatched bars (+/f), n=10] and *Fa2h*$^{flox/flox}$ Cnp1-Cre mice [white bars (f/f), n=6]. No significant difference was observed

between the two groups for both Initial ($p>0.05$) and Reverse ($p>0.05$). (E) TLC analysis of brain galactolipids from *Fa2h*$^{+/flox}$ Cnp1-Cre (+/f) and *Fa2h*$^{flox/flox}$ Cnp1-Cre (f/f) mice. Total brain lipids were extracted from two 10-week-old *Fa2h*$^{flox/flox}$ Cnp1-Cre mice and their respective littermates. Lipids were separated on a HPTLC plate along with GalCer standards and visualized by primuline staining and UV illumination. (F) Mass spectrometry analysis of brain galactolipids from 3-month-old *Fa2h* deficient mice and normal littermates. Individual lipids (12 distinct GalCer and 11 distinct hFA-GalCer) in whole brain lipid extracts obtained from *Fa2h*$^{+/-}$, *Fa2h*$^{-/-}$, *Fa2h*$^{+/flox}$ Cnp1-Cre, and *Fa2h*$^{flox/flox}$ Cnp1-Cre mice (n=2 for each genotype) were measured by LC/MS/MS. The mean and range of the total GalCer (nFA) and hFA-GalCer (hFA) are shown. The values for individual molecular species in each animal are included in Supplementary Table 2.

Table 1

Electrophysiologic parameters of sciatic nerves of 12-month-old *Fa2h*$^{-/-}$ and *Fa2h*$^{+/+}$ mice.

Electrophysiological parameter	*Fa2h*$^{-/-}$ (n=3)	*Fa2h*$^{+/+}$ (n=4)	P value
CMAP distal latency (ms)	0.867 ± 0.12	0.83 ± 0.13	1.00
CMAP distal amplitude (mV)	5.00 ± 1.9	6.03 ± 3.4	0.28
CMAP proximal amplitude (ms)	4.63 ± 1.8	4.88 ± 2.3	0.30
Motor nerve conduction velocity (m/s)	41.3 ± 2.5	43.5 ± 0.58	0.27

The values were compared by paired Student's t-test using Prism 5 (GraphPad Software). Data are expressed as mean ± SD. CMAP, compound motor action potential.